Interpreting Inorganic Compositional Depth Profiles to Understand the Rate-Limiting Step in Vapor Phase Infiltration Processes

Shuaib A. Balogun¹, Yi Ren², Ryan P. Lively² and Mark D. Losego^{1,*}

¹School of Materials Science and Engineering, Georgia Institute of Technology, Atlanta, GA, USA ²School of Chemical and Biomolecular Engineering, Georgia Institute of Technology, Atlanta, GA,

USA

*electronic mail: losego@gatech.edu

Abstract

Vapor phase infiltration (VPI) is a post-polymerization modification technique that infuses inorganics into polymers to create organic-inorganic hybrid materials with new properties. Much is yet to be understood about the chemical kinetics underlying the VPI process. The aim of this study is to create a greater understanding of the process kinetics that govern the infiltration of trimethyl aluminum (TMA) and TiCl₄ into PMMA to form inorganic-PMMA hybrid materials. To gain insight, this paper initially examines the predicted results for the spatiotemporal concentrations of inorganics computed from a recently posited reaction-diffusion model for VPI. This model provides insight on how the Damköhler number (reaction versus diffusion rates) and non-Fickian diffusional processes (hindering) that result from the material transforming from a polymer to a hybrid can affect the evolution of inorganic concentration depth profiles with time. Subsequently, experimental XPS depth profiles are collected for TMA and TiCl₄ infiltrated PMMA films at 90 °C and 135 °C. The functional behavior of these depth profiles at varying infiltration times are qualitatively compared to various computed predictions and conclusions are drawn about the mechanisms of each of these processes. TMA infiltration into PMMA appears to transition from a diffusion-limited process at low temperatures (90 °C) to a reaction-limited process at high temperatures (135 °C) for the film thicknesses investigated here (200 nm). While TMA appears to fully infiltrate these 200 nm PMMA films within a few hours, TiCl₄ infiltration into PMMA is considerably slower, with full saturation not occurring even after 2 days of precursor exposure. Infiltration at 90 °C is so slow that no clear conclusions about mechanism can be drawn; however, at 135 °C, the TiCl₄ infiltration into PMMA is clearly a reaction-limited process, with TiCl₄ permeating the entire thickness (at low concentrations) within only a few minutes, but inorganic loading continuously increasing in a uniform manner over a course of 2 days. Nearsurface deviations from the uniform-loading expected for a reaction-limited process also suggest that diffusional hindering is high for TiCl₄ infiltration into PMMA. These results demonstrate a new, ex situ analysis approach for investigating the rate-limiting process mechanisms for vapor phase infiltration.

1. Introduction

Vapor phase infiltration (VPI) occurs by exposing an organic polymer to an inorganic chemical vapor that sorbs into, diffuses throughout, and eventually becomes "entrapped" within a polymer. Entrapment occurs by the inorganic precursor reacting with the polymer or losing its volatility after reacting with a co-reactant.[1] Competitions between diffusional processes and reaction or transient binding to polymer functional groups influence the overall rate kinetics of the VPI process. Infiltration of trimethylaluminum (TMA) into PMMA to form AlO_xH_y-PMMA hybrids has been extensively studied and has been shown to improve the chemical stability of various polymers.[2] Additionally, TMA has been used in combination with other polymers and block co-polymers to add photoluminescence, photovoltaic, antireflection, filtration and oil sorption properties.[3-10] Fewer studies have focused on the vapor infiltration of titanium-containing precursors into polymers. However, existing reports suggest that vapor infiltration of TiO_x into polymers can improve chemical separations, mechanical strength, and lithographic patterning.[7, 11, 12]

The loading, binding, and temporal mass uptake of inorganic material into the parent polymer has been extensively studied in the TMA/PMMA polymer system. The current understanding is that at low temperatures (< 100 °C), a reversible adduct forms between the TMA precursor and the carbonyl functional groups of PMMA, but a primary chemical bond does not form readily. At higher temperatures (> 100 °C) a reaction occurs between TMA and the carbonyl groups to form C-O-Al bonds between the organic and inorganic components. [13-15]. TMA infiltration into PMMA is thought to be a diffusion-limited process, [2, 16-18] although prior work has shown a change in the activation energy of effective diffusivity above process temperatures of 100 °C, and it has been suggested that this change in activation energy is a consequence of increased reaction rates. [16] Infiltration of most precursors into most polymers is also thought to occur via a diffusion-limited process, although many of these studies focus on TMA. [2, 4, 7, 9, 17-23]

Further studies of fundamental infiltration kinetics in various precursor/polymer systems are needed to build a better understanding of how precursor and polymer chemistry combine to influence the various processes of sorption, diffusion, and reaction and thereby affect the total VPI process kinetics. Compared to TMA, far fewer studies exist on the fundamental process kinetics of TiCl₄ infiltration into PMMA.[24, 25] Sinha *et al.* demonstrated that TiCl₄ diffusivity in PMMA increases with increased process temperatures but posited that as TiCl₄ loading increased, complexation between TiCl₄ and PMMA creates "blockages" that begin to hinder the diffusivity in a non-Fickian manner.[25] Peng *et al.* hypothesized PMMA nanodomains in PS-PMMA block co-polymers serve as reaction sites for the TiCl₄. These researchers observed decreases in TiCl₄ diffusivity with each cycle, supporting this non-Fickian binding and hindering hypothesis.[24] These studies have suggested that TiCl₄ diffuses into PMMA and may react with PMMA, but the extent of loading and rates of diffusion are lower than those for TMA in PMMA. However, the full process kinetics are still not understood for this system.

Recently, a reaction-diffusion model was proposed in an attempt to capture the complex interplay of the processes—sorption, diffusion, and reaction—that occur during vapor infiltration. [26]. This model is based upon Fick's second law and incorporates a second-order chemical reaction term to account for immobilization of infiltrated precursors due to their reaction with or semi-permanent binding to chemical functional groups on the polymer. This model also includes a non-Fickian diffusional hindering term that alters the precursor's diffusivity as precursor-polymer reactions occur and the material transforms from a polymer to a hybrid. When reduced,

the reaction-diffusion model reveals several dimensionless parameters including $\frac{C_S}{C_{nolvmer}^o}$, the

Damköhler number (Da), and the hindering factor ($K' \cdot C_{polymer}^o$). $\frac{c_s}{c_{polymer}^o}$ describes the ratio of

equilibrium surface concentration of physically sorbed precursors to the amount of polymer functional groups that would react with the precursor. This ratio can be adjusted experimentally by varying the precursor partial pressure above the polymer, as this partial pressure is directly correlated to the equilibrium surface concentration of physically dissolved precursors, such as via Henry's Law. The Damköhler number (Da) represents the ratio of the chemical reaction timescale (reaction rate) to the transport phenomena rate (diffusivity) occurring in the system. A high Da signifies a diffusion-limited process in which the reaction rate is much faster than the diffusion rate, while a low Da signifies a reaction-limited process in which the diffusion rate is much faster than the reaction rate. Finally, the hindering factor, $K' \cdot C_{polymer}^o$, accounts for the reduction in diffusivity of sorbed species as a function of immobilized precursor. Ren *et al.* demonstrated that this model could successfully explain and predict the infiltration kinetics for the TMA/PMMA system. Additionally, Jean *et al.* showed how this model could be used to predict and quantify the effects of TMA exposure pressure on the infiltration kinetics and inorganic loading of PIM-1. [27]

In this study, we apply the outputs of this reaction-diffusion model to better understand the rate-limiting mechanisms for VPI of TMA and TiCl₄ into PMMA based upon inorganic compositional depth profiles collected ex-situ after infiltration. To our knowledge, this is the first time that these mechanisms are being determined for a VPI process by comparing the outputs of this model to experimental compositional depth-profile measurements. Specifically, we show how different functional features of the compositional depth profile are indicative of various process mechanisms, including Damköhler number and diffusional hindering. This demonstration provides a new tool for assessing the kinetic mechanisms of VPI processes and demonstrates the differences in mechanism for the TMA and TiCl₄ infiltration processes at varying temperatures.

2. Experimental Methods

PMMA Films

Polymethyl methacrylate (PMMA) was purchased from PolySciences Inc. (\sim 75 kDa molecular weight) and made into a 5 wt.% solution in toluene (anhydrous, 99.8%, Sigma-Aldrich). This solution was spun cast onto silicon substrates at 3000 RPM for 30 s to give films of 160-200 nm nominal thickness. All films were then placed on a hot plate heated to 150 °C for 1 h to remove any remaining solvent.

Vapor Phase Infiltration

PMMA films were infiltrated in a custom-built reactor having a 28 L chamber and operated with decision-tree-based control software.[26] PMMA was infiltrated at process temperatures of 90 °C and 135 °C for TMA and TiCl4. Both precursors were infiltrated with overpressures of ~ 1 Torr. All pressures in the reaction chamber were measured with a Baratron capacitance manometer. All VPI processes used a single precursor / co-reactant cycle with a static hold scheme. The general process sequence performed was (1) ultrahigh purity N₂ gas was flowed into the reactor to purge the system for 5 min, (2) the system was pumped down to base vacuum (30 mTorr) for an hour to remove most water, (3) the chamber was isolated, (4) the precursor valve, which is connected directly to the chamber, was opened for 3 s for TMA or 5 s for TiCl₄ to reach a vapor pressure of

about 1 Torr of precursor (both precursors sources are at room temperature), (5) the precursor was then held in the chamber for between 1 and 48 hours, (6) the system was then pumped to base vacuum for 5 mins, (7) the water co-reactant valve, which is also connected directly to the chamber and held at room temperature, was opened for 1 s to give a vapor pressure of 1.8 Torr in the chamber, and, (8) the water was held in the chamber between 1-24 hours before purging the system for 60s and venting to atmosphere.

X-ray Photoelectron Spectroscopy (XPS)

XPS was performed using a Thermo K-alpha system using a monochromatic Al-Kα X-ray source (1486.6 eV) with a 60° incident angle and a 90° emission collection geometry. Survey scans were conducted at a pass energy of 200 eV and for binding energies from -10 to +1350 eV. For the elemental analysis, the following elements at the following binding energies were collected: Ti 2p (448–475 eV), O 1s (525–545 eV), C 1s (279–298 eV), Cl 2p (190–210 eV) and Si 2p (95–110 eV). Films were etched over a raster size of 400 x 400 mm with a monatomic argon ion gun at a voltage of 2000 V and a high current for 65 seconds, yielding an approximate rate of 25 nm per etch level. At each level the elemental analysis and survey scan was performed. A Shirley background subtraction was used for determining atomic percentages.

Spectroscopic Ellipsometry.

Film thicknesses were measured with an Alpha-SE spectroscopic ellipsometer (J.A. Woollam) at a 70° angle over a spectral range of 340 to 900 nm. The refractive index was fit to a Cauchy model.

3. Results and Discussion

Calculated Predictions of Spatiotemporal Inorganic Concentrations from the Reaction-Diffusion Model

The reaction-diffusion model calculates the spatiotemporal distributions of infiltrated precursors inside the polymer during VPI. Specifically, the model outputs concentrations for two different populations of infiltrated precursors species: (1) precursors that have "reacted" with the polymer functional groups ($C_{product}$) and (2) precursors that are dissolved and freely diffusing in the polymer but have yet to react with the polymer (C_{free}). The sum of these two concentrations is the total concentration of inorganic precursors within the polymer (C_{total}).

Fig. 1 schematically illustrates these concentrations for diffusion-limited and reaction-limited processes. Note the starting conditions here assume a fixed concentration of polymer functional groups ($C_{polymer}^o$) with which the precursor could react and a solubility limit for dissolution of the inorganic precursor into the polymer (C_s), which is assumed to be the dissolved concentration at the surface at all times. Upon infiltration, precursors either remain dissolved (lighter green) or bind/react with the polymer functional group (dark green), consuming the polymer functional groups. Note that both routes achieve a similar final state ("fully infiltrated") but follow different spatiotemporal distribution pathways to achieve that state. Note that as reactions occur, the remaining concentration of unreacted polymer functional groups is denoted as $C_{polymer}$ such that the initial concentration of unreacted functional groups $C_{polymer}^o = C_{polymer} + C_{product}$, thus denoting the extent of reaction.

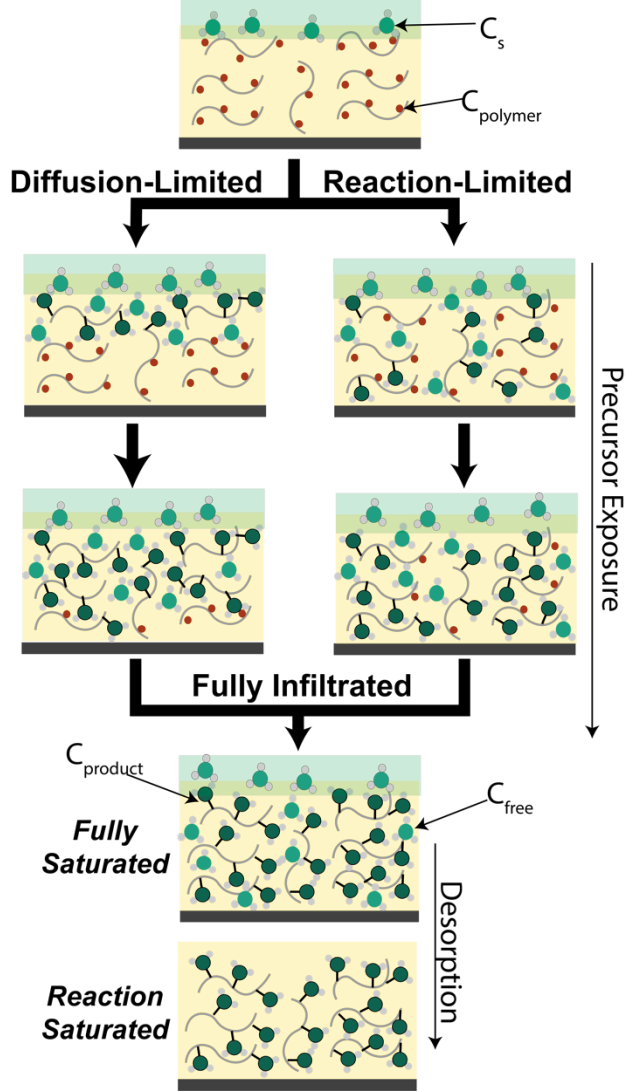


Fig. 1: Schematic illustration of diffusion- and reaction-limited pathways in a vapor phase infiltration process.

Before considering each process path individually, let us define what "saturation" can mean in this system. Two types of "saturation" can be considered: (1) reaction saturation occurs when the infiltrated inorganic precursor has reacted with all of the available polymer functional groups, $C_{product} = C_{polymer}^o$ [reaction saturation] and (2) full saturation occurs when both all of the functional groups are reacted and the polymer/hybrid has reached its saturation limit for dissolution of freely dissolved inorganic precursors, at which point, $C_{product} = C_{polymer}^o$ and $C_{free} = C_s$ throughout the entire polymer, such that $C_{total} = C_{polymer}^o + C_s$ [reaction + dissolution saturation]. As depicted in **Fig. 1**, full saturation nominally occurs during process completion when a precursor overpressure is present to keep precursors dissolved, while reaction saturation is expected to be the condition if dissolved species are permitted to fully desorb prior to introduction of the coreactant.

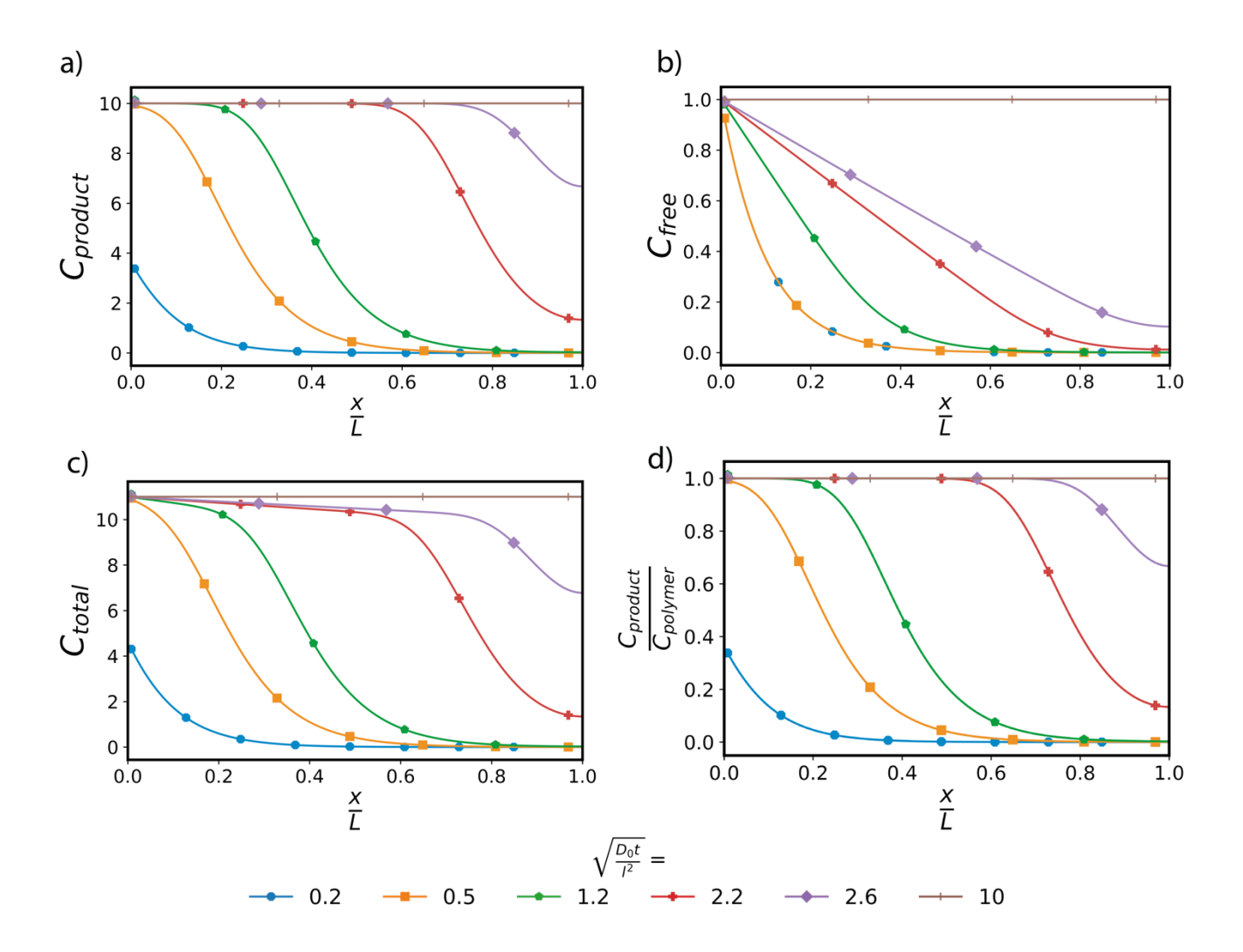


Fig. 2: Depth profiles of inorganic concentrations at varying precursor exposure times $(\sqrt{\frac{D_0 t}{l^2}})$ using the reaction-diffusion mode where x/L is a normalized infiltration depth given that L is the film's thickness. Here, four different representations of the inorganic concentration are presented for the exact same process conditions: (a) the concentration of reacted inorganic product, $C_{product}$, (b) the concentration of freely dissolved inorganic precursors, C_{free} , (c) the sum total of reacted and freely dissolved precursors, C_{total} , and (d) the ratio of the concentration of reacted precursors to the total concentration of possible reaction sites, $C_{product}/C_{polymer}^o$. For these calculations, Da = 100, $C_s = 1$, $C_{polymer}^o = 10$ and $K' \cdot C_{polymer}^o = 0.5$.

Fig. 2 plots the outputs of the reaction-diffusion model for a diffusion-limited case (Da = 100). This figure explicitly plots the different types of inorganic concentrations that can be calculated from the model: (a) $C_{product}$, (b) C_{free} , and (c) C_{total} . Note that the dimensionless exposure time $(\sqrt{\frac{D_0 t}{l^2}})$ represents a ratio between the characteristic diffusion length $(\sqrt{D_0 t})$ and the film's thickness (l), and thus a value of 1 represents a characteristic time for most precursors to diffuse to the depth of the film's thickness assuming Fickian behavior. Here, we have set $C_s = 1$ and $C_{polymer}^o = 10$ such that the non-dimensional parameter $C_s/C_{polymer}^o$ is 0.1, the maximum $C_{product}$ is 10 (**Fig. 2a**), and the maximum C_{free} is 1 (**Fig. 2b**). $K' \cdot C_{polymer}^o$ was set to 0.5. To create more general plots, these concentrations can be normalized to a relevant reference concentration, as was

done in Ren *et al.* [26], but the unnormalized plots are instructive in understanding the behavior of the different populations of infiltrated inorganic. For example, $C_{product}$ in **Fig. 2a** resembles a moving boundary case – albeit not entirely abrupt – in which all functional groups behind the boundary are reacted and all polymer functional groups beyond the boundary are unreacted. In contrast, C_{free} in **Fig. 2b** resembles a purely Fickian diffusion behavior with the surface concentration fixed at the solubility limit and no other depth reaching saturation until completion. **Fig. 2c** is the linear addition of $C_{product}$ and C_{free} , with a saturation value of $C_s + C_{polymer}^o = 1 + 10 = 11$.

For physical experiments, like the ones presented subsequently, precursor infiltration can be followed by a long "purge" step in which the inorganic precursor overpressure is removed, and the freely diffusing precursors (C_{free}) are permitted to out-diffuse and desorb.[2] In the ideal case, this physical experiment should leave a compositional depth profile similar to just the $C_{product}$ population. This $C_{product}$ can be normalized with respect to the concentration of polymer functional groups, $C_{polymer}^o$ to quantify the percentage of reaction saturation achieved. This normalized compositional profile is plotted in **Fig. 2d** and will be the concentration profile used in subsequent model calculations because of its physical relevance to the data presented here. Note that its functional form is identical to **Fig. 2a**.

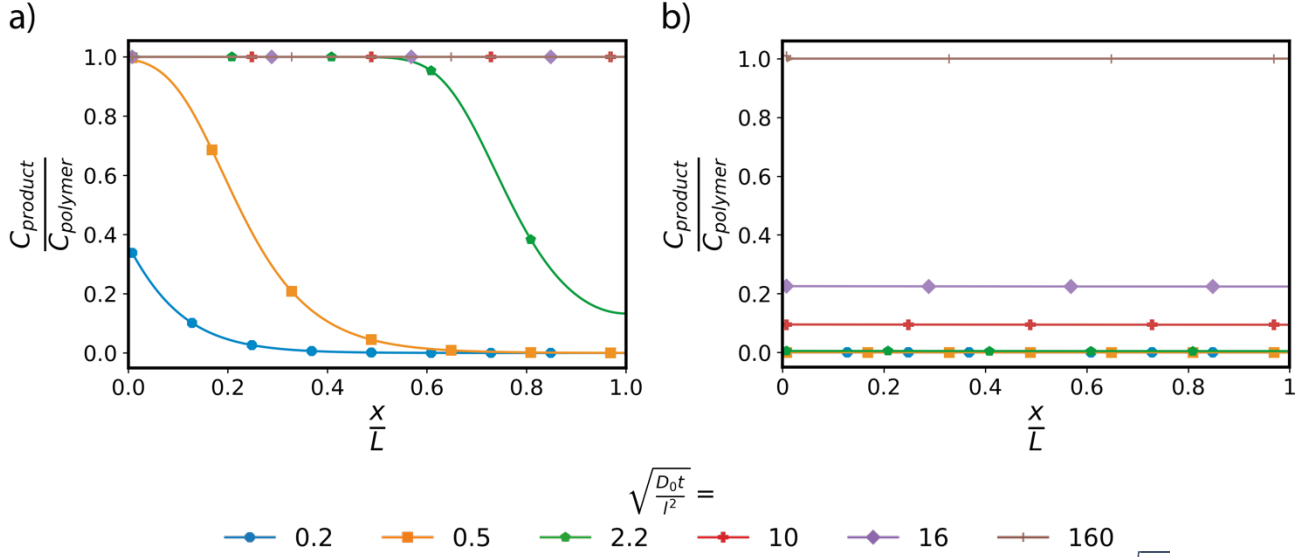


Fig. 3: Depth profiles of inorganic concentration calculated at varying precursor exposure times $(\sqrt{\frac{D_0 t}{l^2}})$ using the reaction-diffusion model for (a) a system with a Damköhler number of 100 (diffusion-limited) and (b) a system with a Damköhler number of 0.01 (reaction-limited). $C_{product}/C_{polymer}^o$ is the concentration of functional groups in the polymer that have reacted with the infiltrated precursor, with a value of 1 representing 100% of the polymer's functional groups having reacted with an infiltrated precursor. x/L is the normalized infiltration depth, where L is the film thickness. In all cases, the diffusion hindering, $K' \cdot C_{polymer}^o$, is set to be 0.5

Next, we return to the two different rate-limiting pathways introduced in **Fig. 1**. **Fig. 3** compares computed results of spatiotemporal inorganic loading for a diffusion-limited (**Fig. 3a**, Da = 100) versus reaction-limited (**Fig. 3b**, Da = 0.01) case. These results are nominally identical to what was first published by Ren *et al.* [26], except that they describe the unidirectional case rather than the bidirectional diffusion case. The mass uptake is again normalized to the number of

functional groups available in the polymer as was done in **Fig. 2d** such that reaction saturation occurs when this ratio equals 1. This figure demonstrates the distinct difference in spatial concentrations of reacted inorganics for a diffusion-limited (**Fig. 3a**) versus reaction-limited (**Fig. 3b**) infiltration process. While the diffusion-limited process exhibits a sigmoidal-type of profile that marches deeper into the polymer depth with time, the reaction-limited condition exhibits a nearly constant concentration of reacted species into the film depth. For the simulation conditions chosen here, this uniform concentration requires a significant amount of time to rise above zero $(\sqrt{\frac{D_0 t}{l^2}} > 2.2)$ before then monotonically increasing to the same reaction saturation concentration as the diffusion-limited process, as was illustrated in **Fig. 3** (same end state).

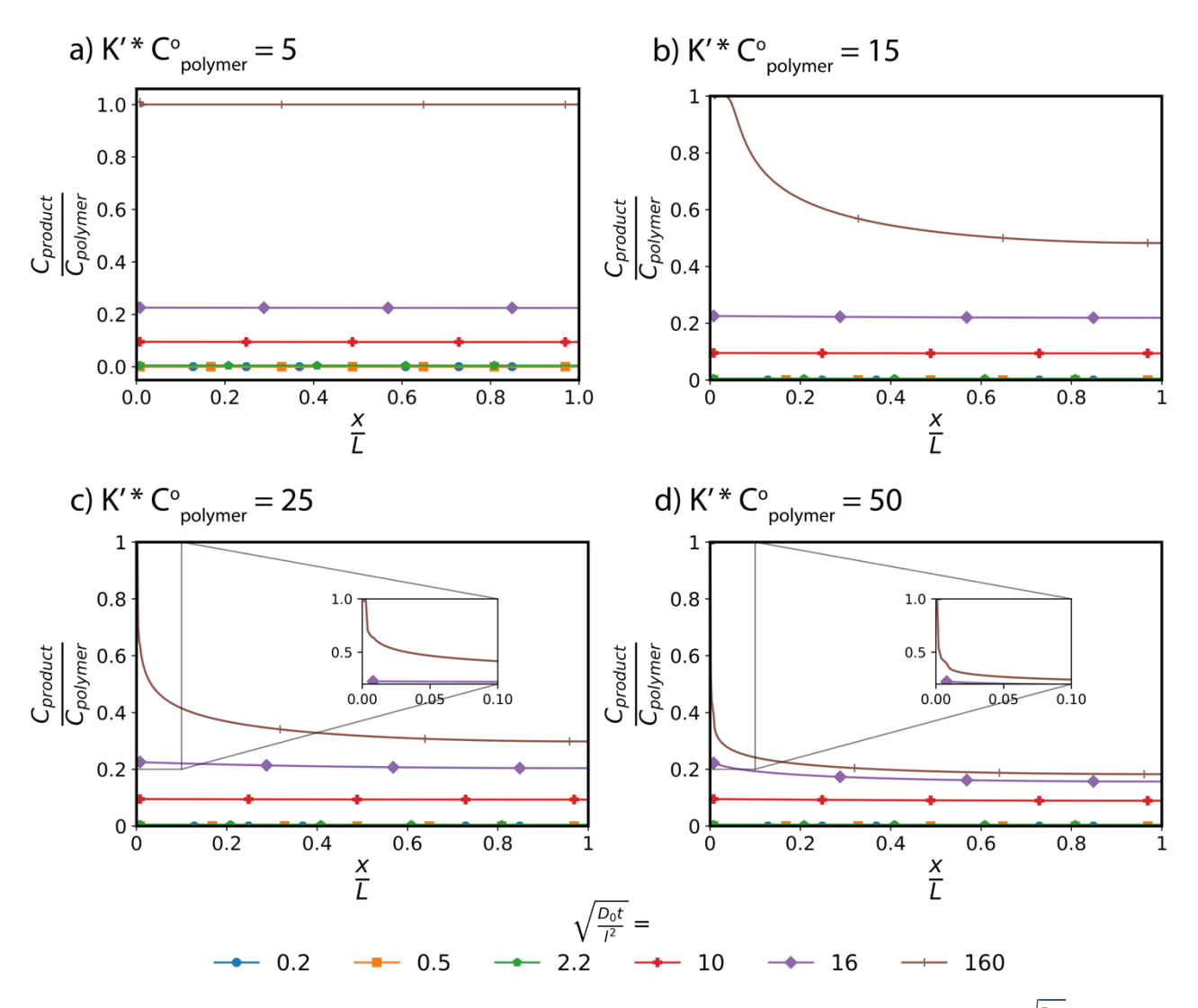


Fig. 4: Depth profiles of inorganic concentration calculated at varying precursor exposure times $(\sqrt{\frac{D_0 t}{l^2}})$ using the reaction-diffusion model for reaction-limited systems (Da = 0.01) with varying diffusional hindering parameters: (a) K'·C°_{polymer} = 5, (b) K'·C°_{polymer} = 15, (c) K'·C°_{polymer} = 25, (d) K'·C°_{polymer} = 50. C_{product}/C_{polymer} is the concentration of functional groups in the polymer that have reacted with the infiltrated precursor, with a value of 1 representing 100% of the polymer's functional groups having reacted with an infiltrated precursor. x/L is the normalized infiltration depth, where L is the film thickness.

A second mechanism that can alter the spatiotemporal composition profile during infiltration is non-Fickian diffusion. In the reaction-diffusion model the use of a concentration-dependent hindering parameter attempts to capture some of this non-Fickian transport resulting from changes in diffusivity as the polymer transforms to a hybrid material. Specifically, in the reaction-diffusion model, the diffusivity is set to be a function of the concentration of reacted precursors, C_{product} , such that $\frac{D}{D_0} = \exp(-K' \cdot C_{\text{product}})$. Note that C_{product} is a function of time, increasing as more of the infiltrated precursor reacts with the polymer's functional groups. Nominally, this concentration-dependent diffusivity could even be used to capture changes in diffusivity for subsequent infiltration cycles if a multi-cycle process were to be used.

To better understand how this hindering may affect compositional depth profiles, **Fig. 4** presents computed profiles at varying hindering parameters ($K' \cdot C^o_{polymer}$ values from 5 to 50) for a reaction-limited process (Da = 0.01). At low hindering ($K' \cdot C^o_{polymer} = 5$, **Fig. 4a**) concentration profiles are uniform at all times. However, as the hindering factor increases, concentrations deviate from this uniform depth profile. While short exposure times still exhibit uniform spatial loading, longer exposure times lead to a rise in concentrations near the polymer's surface. These results suggest that hindering effects may also be detectable in spatiotemporal inorganic compositional profiles of VPI treated materials.

Experimental Results for TMA and TiCl₄ Infiltration into PMMA films on Silicon

XPS with ion sputtering is used to collect inorganic compositional depth profiles for PMMA films on silicon substrates that are vapor phase infiltrated with TMA or TiCl₄ at varying precursor exposure times. Subsequently, these compositional profiles are qualitatively compared with the profiles computed from the reaction-diffusion model, as presented above. Several limitations are recognized in this experiment-to-model comparison. First, we assume that the profile of reacted species stays constant with subsequent process steps including purging and coreaction with water. Further, measurement errors are likely introduced from sputter damage during depth profiling. However, as will be shown, the experimental results are largely consistent in functional form to the phenomenological predictions of the reaction-diffusion model and appear indicative of the mechanisms that are rate-controlling infiltration in these system.

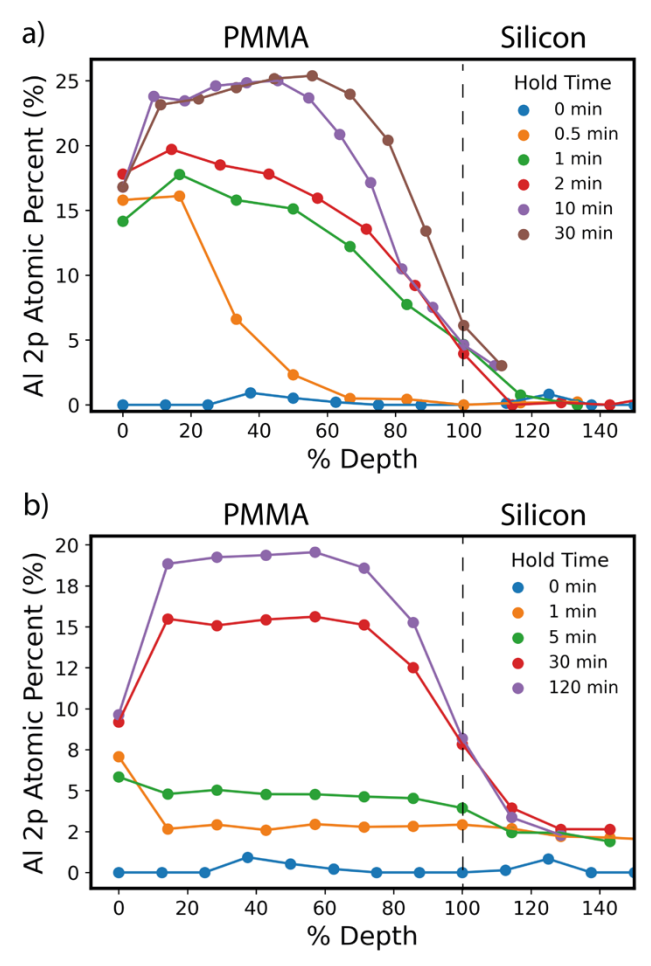


Fig. 5: XPS depth profiles collected from PMMA films infiltrated with TMA + H_2O at (a) 90 °C processing temperature and (b)135 °C processing temperature at varying exposure times of the inorganic precursor, 0 to 30 mins for the 90 °C process and 0 to 120 min for the 135 °C process. All films are nominally 200 nm thick, but depth is normalized to the silicon substrate signal (not shown for clarity).

Fig. 5 presents Al 2p XPS depth profiles for TMA infiltrated into 200 nm PMMA films on silicon at 90 °C (Fig. 5(a)) and 135 °C (Fig. 5(b)) at varying infiltration times. The ordinate axis has been normalized to the total film thickness based upon the silicon substrate signal to improve comparisons amongst each film. The thickness normalization can be reviewed in Fig. S1; in general films varied by less than 10% in thickness. TMA infiltration into PMMA occurs quite readily at the process temperature of 90 °C and 135 °C, on time scales of just a few minutes (0 to 5 mins). Noticeable here is the marked difference in the functional form of the concentration depth profiles between the two process temperatures. At 90 °C (Fig. 5(a)) the inorganic concentrations resemble diffusion-limited profiles, with maximum inorganic concentration at the surface at all infiltration times and a sigmoidal decline into the material bulk. This decline reaches near zero at the silicon interface for low infiltration times but raises towards the maximum concentration with increased infiltration times. This behavior approximates the diffusion-limited spatiotemporal concentrations that the reaction-diffusion model predicts in Fig. 3a. This observation of diffusionlimited behavior is also consistent with prior reports for TMA infiltration into PMMA. [2, 15, 17-21, 26] Note that for these conditions, saturation of ~ 25 at% aluminum is achieved after only 10 min of TMA exposure.

In contrast, at 135 °C (Fig. 5b), we observe different functional forms for the spatiotemporal inorganic profiles and, hence, an apparently different rate-limiting mechanism. At low infiltration times the Al concentration is relatively uniform through the film thickness. While this uniform concentration deviates some at longer hold times (30 and 120 min), we suspect this has more to do with measurement limitations or possible hindering rather than a change in mechanism. Interestingly, this uniform compositional profile behavior resembles the reaction-limited profile of Fig. 3(b). At first, this result may seem somewhat surprising; it suggests that the TMA diffuses through the entire thickness before reacting, which seems to contradict other known reports. This result suggests that diffusion occurs rather quickly in this system but the "reaction" necessary for entrapment of the TMA species within the PMMA films is much slower. It is known that at higher temperatures TMA forms a permanent covalent bond with PMMA's carbonyl rather than just the adduct formed at lower temperatures. Therefore, it is possible that due to the higher energy needed to form the covalent bond the mechanism of infiltration changes from diffusion-limited to reactionlimited [2, 15, 19-23]. A second possibility to consider is that PMMA's glass transition temperature is ~105°C and this transition from a glassy to rubbery state may enhance diffusivity, leading to a reaction-limited process at higher temperatures. What is clearly consistent between the observations made here and those reported previously is that a change in mechanism occurs for processes below and above about 100 °C. [16]

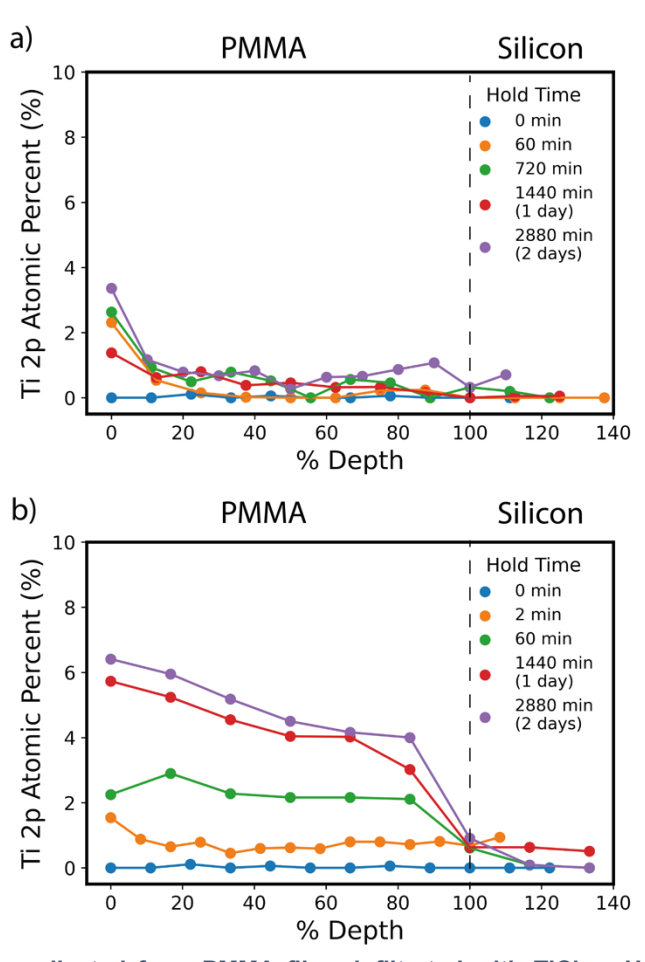


Fig. 6: XPS depth profiles collected from PMMA films infiltrated with $TiCl_4 + H_2O$ at a) 90 °C processing temperature at varying exposure times of the inorganic precursor. (a) $TiCl_4$ infiltration was carried out at 90 °C at hold times varying from 0 to 2880 mins. (b) $TiCl_4$ infiltration was

carried out at 135 °C for hold times varying from 0 to 2880 mins. All films are nominally 200 nm thick, but depth is normalized to the silicon substrate signal (not shown for clarity).

Next, we turn to examine the behavior of TiCl₄ infiltration into PMMA. From the atomic layer deposition (ALD) literature, TiCl₄ is known to be less reactive towards oxidants than TMA, often resulting in reaction-limited processes. [28, 29] Fig. 6 presents XPS depth profiles for Ti 2p at TiCl₄ infiltration temperatures of 90 °C (Fig. 6(a)) and 135 °C (Fig. 6(b)) into 200 nm PMMA films at varying precursor exposure times. At 90 °C, minimal titanium (< 2%) is infiltrated into the films at all exposure times up to 2880 min (2 days). Note that these timescales are significantly longer than those explored in Fig. 5 for TMA infiltration into PMMA (maximum of 120 min). This difference in times is indicative of the much slower infiltration kinetics for TiCl₄ compared to TMA. As TiCl₄ exposure time increases (0 to 2880 mins), the surface concentration of titanium increases (0 to ~4 at%), however the sub-surface concentration increases much more slowly. At 60 mins of TiCl₄ exposure, no titanium exists beyond about 20% depth from the surface (~40 nm). As exposure time increases, we begin to detect Ti throughout the entire depth. However, the low concentrations relative to experimental noise make it difficult to determine the functional forms of these depth profiles. Arguably TiCl₄ exposure times of 60, 720, and 1440 min appear to have decreasing concentrations resembling a diffusion-limited profile while the 2-day exposure resembles somewhat uniform loading with depth. However, clear conclusions on mechanism cannot be made. What is clear is the significantly slower overall VPI process kinetics for TiCl₄ versus TMA infiltration into PMMA, consistent with what has previously been reported.[24, 25]

At the higher infiltration temperature of 135 °C, shown in Fig. 6b, TiCl₄ does infiltrate into PMMA within reasonable process times. At this higher temperature, inorganic depth profiles show relatively uniform concentrations throughout the film thickness that increase monotonically with exposure time, especially from 0 to 60 min of infiltration. This uniform depth profile is indicative of a reaction-limited infiltration process, as illustrated in Fig. 3b. It is notable that although total infiltration kinetics are slow in this system because the process is now within a reaction-limited regime, the titanium is detected throughout the entire depth even at only 2 min of TiCl₄ exposure time – diffusion is clearly not the limiting factor. This result is consistent with prior studies that report rapid sorption of TiCl₄ into PMMA via in situ quartz crystal microbalance (QCM) gravimetry, indicative of a high diffusivity that is not hindered by reaction.[24, 25] At 1-day and 2-days of exposure, concentration profiles deviate from uniformity within the near surface region where inorganic concentration rises. We attribute the development of this increased near-surface concentration to diffusional hindering effects. As illustrated in Fig. 4b-d, hindering can lead to increases of near-surface concentrations of inorganics for reaction-limited processes as exposure time increases, and we interpret this feature at these longer exposure times as indicative of this We postulate that TiCl₄'s larger molecular size than TMA may be causing this increased hindering, although further studies are warranted to understand this phenomenon more directly.

Summary and Implications of Results

These experimental results demonstrate how differences in chemistry and process temperature alter the VPI process kinetics and how the reaction-diffusion model can be used to interpret experimental results. Understanding the fundamental chemical kinetics is important in process scale-up, but as shown in this study, these differences in process kinetics can also influence the final spatial distributions of inorganics in the resultant hybrid material. For example, the diffusion-limited profiles (like TMA infiltration into PMMA at low temperatures) can produce

near-surface loaded inorganic compositions at low process times, while reaction-limited conditions (like TiCl₄ infiltration into PMMA at high temperatures) can produce uniform inorganic loading throughout the entire sample's depth, with monotonically increasing concentration over extended exposure times. These differences in inorganic distribution could be important depending upon the material's specific application. For example, these differences in spatial distribution could have direct implications for controlling ceramic nanostructures that can be formed via pyrolysis of the infiltrated hybrid materials. It is also worthwhile to note that the kinetics of the infiltration process will continue to change if subsequent infiltration cycles are used. The continued change in the infiltrated materials' chemistry will likely continue to affect diffusivity and reactivity of the infiltrating precursors. Furthering the understanding of infiltration process kinetics will continue to provide new insights into how this process can be used to control the chemical structure of infiltration-synthesized organic-inorganic hybrid materials.

4. Conclusions

Combining the reaction-diffusion model outputs with experimental ex situ compositional inorganic depth profiling data provides insights into the mechanisms of vapor phase infiltration processes. Specifically, we demonstrate both computationally and experimentally that diffusionlimited VPI processes will have sigmoidal depth profiles while reaction-limited VPI processes will have uniform concentrations of inorganic throughout the polymer's depth. These inorganic concentration profiles can be further altered by non-Fickian diffusional hindering that results from changes in the material's diffusivity as it transforms from a polymer to a hybrid material. This paper has specifically examined TMA and TiCl₄ infiltration into 200 nm thick PMMA films at two different temperatures, 90 °C and 135 °C. TMA appears to transition from a diffusion-limited process to a reaction-limited process at this film thickness as the process temperature is increased. In contrast, TiCl4 infiltration into PMMA is incredibly slow at 90 °C, with less than 2 at% Ti infiltrated into the film's bulk within even 2 days of precursor exposure, making it difficult to make any conclusion about process mechanisms. At 135 °C, while still significantly slower than TMA, the TiCl₄ process is clearly reaction-limited, exhibiting inorganic concentration profiles that are uniform with depth. Interestingly, because the process is reaction-limited and diffusion is presumably fast, Ti is detected throughout the entire film's depth (200 nm) after only 1 min of precursor exposure. However, the infiltrated concentration continues to rise for up to 2 days of TiCl₄ exposure. Eventually, deviations from composition depth uniformity emerge, indicative of diffusional hindering. These results demonstrate how an understanding of process mechanism can be used to create different spatial profiles of inorganics in a polymer using an infiltration process. This control over spatial distribution is an important tool in the chemical design of these hybrid materials.

5. Conflicts of Interest

There are no conflicts to declare.

6. Acknowledgements

This material is based upon work supported by the National Science Foundation Graduate Research Fellowship under Grant No. DGE-2039655 and by the NSF program Designing Materials to Revolutionize and Engineer our Future (DMREF-1921873). Any opinion, findings, and conclusions or recommendations expressed in this material are those of the authors(s) and do not necessarily reflect the views of the National Science Foundation. This work was also supported by the Laboratory Directed Research and Development program at Sandia National Laboratories, a multimission laboratory managed and operated by National

Technology and Engineering Solutions of Sandia LLC, a wholly owned subsidiary of Honeywell International Inc. for the U.S. Department of Energy's National Nuclear Security Administration under contract DE-NA0003525. This work was also performed in part at the Georgia Tech Institute for Electronics and Nanotechnology, a member of the National Nanotechnology Coordinated Infrastructure (NNCI), which is supported by the National Science Foundation (ECCS-2025462).

References

- [1] C.Z. Leng, M.D. Losego, Vapor phase infiltration (VPI) for transforming polymers into organic–inorganic hybrid materials: a critical review of current progress and future challenges, Materials Horizons 4 (2017) 747-771.
- [2] E.K. McGuinness, C.Z. Leng, M.D. Losego, Increased Chemical Stability of Vapor-Phase Infiltrated AlOx–Poly(methyl methacrylate) Hybrid Materials, ACS Applied Polymer Materials 2 (2020) 1335-1344.
- [3] E. Barry, A.U. Mane, J.A. Libera, J.W. Elam, S.B. Darling, Advanced oil sorbents using sequential infiltration synthesis, Journal of Materials Chemistry A 5 (2017) 2929-2935.
- [4] D. Berman, S. Guha, B. Lee, J.W. Elam, S.B. Darling, E.V. Shevchenko, Sequential infiltration synthesis for the design of low refractive index surface coatings with controllable thickness, ACS nano 11 (2017) 2521-2530.
- [5] A. Rahman, A. Ashraf, H. Xin, X. Tong, P. Sutter, M.D. Eisaman, C.T. Black, Sub-50-nm self-assembled nanotextures for enhanced broadband antireflection in silicon solar cells, Nature communications 6 (2015) 1-6.
- [6] H.I. Akyildiz, K.L. Stano, A.T. Roberts, H.O. Everitt, J.S. Jur, Photoluminescence Mechanism and Photocatalytic Activity of Organic–Inorganic Hybrid Materials Formed by Sequential Vapor Infiltration, Langmuir 32 (2016) 4289-4296.
- [7] E.K. McGuinness, F. Zhang, Y. Ma, R.P. Lively, M.D. Losego, Vapor phase infiltration of metal oxides into nanoporous polymers for organic solvent separation membranes, Chemistry of Materials 31 (2019) 5509-5518.
- [8] J.E. Allen, B. Ray, M.R. Khan, K.G. Yager, M.A. Alam, C.T. Black, Self-assembly of single dielectric nanoparticle layers and integration in polymer-based solar cells, Applied Physics Letters 101 (2012) 063105.
- [9] R.Z. Waldman, D. Choudhury, D.J. Mandia, J.W. Elam, P.F. Nealey, A.B. Martinson, S.B. Darling, Sequential infiltration synthesis of Al2O3 in polyethersulfone membranes, Jom 71 (2019) 212-223.
- [10] C. Zhou, T. Segal-Peretz, M.E. Oruc, H.S. Suh, G. Wu, P.F. Nealey, Fabrication of nanoporous alumina ultrafiltration membrane with tunable pore size using block copolymer templates, Advanced Functional Materials 27 (2017) 1701756.
- [11] C.-Y. Nam, A. Stein, K. Kisslinger, Direct fabrication of high aspect-ratio metal oxide nanopatterns via sequential infiltration synthesis in lithographically defined SU-8 templates, Journal of Vacuum Science & Technology B, Nanotechnology and Microelectronics: Materials, Processing, Measurement, and Phenomena 33 (2015) 06F201.
- [12] S.-M. Lee, E. Pippel, U. Gösele, C. Dresbach, Y. Qin, C.V. Chandran, T. Bräuniger, G. Hause, M. Knez, Greatly increased toughness of infiltrated spider silk, Science 324 (2009) 488-492.

- [13] M. Biswas, J.A. Libera, S.B. Darling, J.W. Elam, New insight into the mechanism of sequential infiltration synthesis from infrared spectroscopy, Chemistry of Materials 26 (2014) 6135-6141.
- [14] E.C. Dandley, C.D. Needham, P.S. Williams, A.H. Brozena, C.J. Oldham, G.N. Parsons, Temperature-dependent reaction between trimethylaluminum and poly(methyl methacrylate) during sequential vapor infiltration: experimental and ab initio analysis, Journal of Materials Chemistry C 2 (2014) 9416-9424.
- [15] G.T. Hill, D.T. Lee, P.S. Williams, C.D. Needham, E.C. Dandley, C.J. Oldham, G.N. Parsons, Insight on the Sequential Vapor Infiltration Mechanisms of Trimethylaluminum with Poly (methyl methacrylate), Poly (vinylpyrrolidone), and Poly (acrylic acid), The Journal of Physical Chemistry C 123 (2019) 16146-16152.
- [16] C.Z. Leng, M.D. Losego, A physiochemical processing kinetics model for the vapor phase infiltration of polymers: measuring the energetics of precursor-polymer sorption, diffusion, and reaction, Physical Chemistry Chemical Physics 20 (2018) 21506-21514.
- [17] N. Sasao, S. Sugimura, K. Asakawa, Metal diffusion model in polymer matrices in vapor phase infiltration, Japanese Journal of Applied Physics 60 (2021) SCCC04.
- [18] R.Z. Waldman, N. Jeon, D.J. Mandia, O. Heinonen, S.B. Darling, A.B.F. Martinson, Sequential Infiltration Synthesis of Electronic Materials: Group 13 Oxides via Metal Alkyl Precursors, Chemistry of Materials 31 (2019) 5274-5285.
- [19] B. Gong, Q. Peng, J.S. Jur, C.K. Devine, K. Lee, G.N. Parsons, Sequential vapor infiltration of metal oxides into sacrificial polyester fibers: shape replication and controlled porosity of microporous/mesoporous oxide monoliths, Chemistry of Materials 23 (2011) 3476-3485.
- [20] H.I. Akyildiz, R.P. Padbury, G.N. Parsons, J.S. Jur, Temperature and exposure dependence of hybrid organic–inorganic layer formation by sequential vapor infiltration into polymer fibers, Langmuir 28 (2012) 15697-15704.
- [21] H.I. Akyildiz, M. Lo, E. Dillon, A.T. Roberts, H.O. Everitt, J.S. Jur, Formation of novel photoluminescent hybrid materials by sequential vapor infiltration into polyethylene terephthalate fibers, Journal of Materials Research 29 (2014) 2817-2826.
- [22] R.P. Padbury, J.S. Jur, Comparison of precursor infiltration into polymer thin films via atomic layer deposition and sequential vapor infiltration using in-situ quartz crystal microgravimetry, Journal of Vacuum Science & Technology A: Vacuum, Surfaces, and Films 32 (2014) 041602.
- [23] R.P. Padbury, J.S. Jur, Temperature-dependent infiltration of polymers during sequential exposures to trimethylaluminum, Langmuir 30 (2014) 9228-9238.
- [24] Q. Peng, Y.-C. Tseng, Y. Long, A.U. Mane, S. DiDona, S.B. Darling, J.W. Elam, Effect of Nanostructured Domains in Self-Assembled Block Copolymer Films on Sequential Infiltration Synthesis, Langmuir 33 (2017) 13214-13223.
- [25] A. Sinha, D.W. Hess, C.L. Henderson, Transport behavior of atomic layer deposition precursors through polymer masking layers: Influence on area selective atomic layer deposition, Journal of Vacuum Science & Technology B: Microelectronics and Nanometer Structures Processing, Measurement, and Phenomena 25 (2007) 1721-1728.
- [26] Y. Ren, E.K. McGuinness, C. Huang, V.R. Joseph, R.P. Lively, M.D. Losego, Reaction—Diffusion Transport Model to Predict Precursor Uptake and Spatial Distribution in Vapor-Phase Infiltration Processes, Chemistry of Materials 33 (2021) 5210-5222.

[27] B.C. Jean, Y. Ren, E.K. McGuinness, R. Lively, M.D. Losego, Effects of trimethylaluminum vapor pressure and exposure time on inorganic loading in vapor phase infiltrated PIM-1 polymer membranes, Materials Chemistry and Physics (2022) 126577. [28] S.A. Gregory, C.P. McGettigan, E.K. McGuinness, D.M. Rodin, S.K. Yee, M.D. Losego, Single-Cycle Atomic Layer Deposition on Bulk Wood Lumber for Managing Moisture Content, Mold Growth, and Thermal Conductivity, Langmuir 36 (2020) 1633-1641. [29] F. Gao, S. Arpiainen, R.L. Puurunen, Microscopic silicon-based lateral high-aspect-ratio structures for thin film conformality analysis, Journal of Vacuum Science & Technology A: Vacuum, Surfaces, and Films 33 (2015) 010601.